

Fourth order time-stepping methods with local discontinuous Galerkin approximation for nonlinear Schrödinger equations

X. Liang^{1,*}, A. Q. M. Khaliq¹, and Y. Xing²

¹ Department of Mathematical Sciences and Center for Computational Science
Middle Tennessee State University, Murfreesboro, TN 37132-0001, USA

² Computer Science and Mathematics Division, Oak Ridge National Laboratory, Oak Ridge, TN 37831 and Department of Mathematics, University of Tennessee, Knoxville, TN 37996

Abstract. This paper studies a local discontinuous Galerkin method combined with fourth order exponential time differencing Runge-Kutta time discretization and a fourth order conservative method for solving the nonlinear Schrödinger equations. Based on different choices of numerical fluxes, we propose both energy-conserving and energy-dissipative local discontinuous Galerkin methods, and have proven the error estimates for the semi-discrete methods applied to linear Schrödinger equation. The numerical methods are proven to be highly efficient and stable for long-range soliton computations. Extensive numerical examples are provided to illustrate the accuracy, efficiency and reliability of the proposed method.

1 Introduction

The N-coupled nonlinear Schrödinger equation (NLSE) is widely used to model a number of important physical phenomena, including propagations of solitary waves in optical fibers [2], deep water turbulence [25] and laser beams [31]. In 1967, the 2-coupled NLSE was first derived in [3] to study two interacting nonlinear packets in a dispersive and conservative system. The N-coupled NLSE was proposed in [28] to accurately evaluate the signal distortion in optical communication fibers, and further studied in many literatures. In one space dimension, it takes the form of

$$iu_{nt} + i\alpha_n u_{nx} + \epsilon_n u_{nxx} + \left(\sum_{m=1}^N \beta_{nm} |u_m|^2 \right) u_n = 0, n = 1, 2, \dots, N, \quad (1.1)$$

*Corresponding author. Email addresses: x12h@mtmail.mtsu.edu (X. Liang)

where u_n represent the amplitude of the pulse envelopes, α_n indicate the group velocities for polarization components, ϵ_n are the group velocity dispersion parameters, and β_{mn} are nonlinearity parameters responsible for the Self Phase Modulation [1].

A vast amount of literature can be found on the numerical approximation of the NLSEs. Many different types of numerical methods, including finite difference, finite element, finite volume, and spectral methods, have been designed, see for example, [7, 15, 18, 20, 21, 29, 30, 32, 34, 36] and references therein. The analysis of some finite difference methods can be found in [7, 20, 34]. Recently, [33] studies a finite difference scheme for 2-coupled NLSEs, and they have shown the boundedness of the numerical solution in the discrete L_∞ norm. The numerical solutions of the NLSEs by both finite element Galerkin and finite difference methods are investigated in [15]. It appears that the Galerkin method produces more acceptable results for a wider range of parameters. Many finite element methods have been studied for the NLSEs, see [21, 29] and the references therein.

However, most articles mentioned above do not consider the group velocity for polarization components, except for [20, 36]. In this paper, we consider (1.1) with $\alpha_n \neq 0$, since α_n has significant meanings in nonlinear fiber optics. According to [1], even a single-mode fiber can support two degenerate modes that are polarized in two orthogonal directions. Especially, in high-birefringence fibers, the group velocity mismatch between the fast and slow components of the input pulse cannot be neglected, which means the polarization components α_n in (1.1) cannot be ignored.

The numerical methods discussed here are the discontinuous Galerkin (DG) methods. They belong to a class of finite element methods using piecewise polynomial spaces for both the numerical solution and the test functions. They were originally devised to solve hyperbolic conservation laws with only first order spatial derivatives, e.g. [11, 13]. They have many attractive advantages, including the allowance of arbitrarily unstructured meshes, a compact stencil and easy h - p adaptivity. The DG methods were later generalized to the local discontinuous Galerkin (LDG) methods by Cockburn and Shu to solve the convection-diffusion equation [12]. As a result, the LDG methods have been successfully applied to solve various partial differential equations (PDEs) containing higher-order derivatives. For the single and 2-coupled NLSEs, a Runge-Kutta LDG method was first developed in [36], in which they provided the stability analysis and a $k+1/2$ -th error estimate for the linearized problem.

The performance of several fourth order temporal discretizations for the single NLSEs is compared in [23]. Methods considered there include the exponential time-differencing fourth-order Runge-Kutta (ETD4RK) method as proposed by Cox and Matthews [14] with implementation by Kassam and Trefethen [22], integrating factors, time-splitting, Fornberg and Driscoll's 'sliders', and an ODE solver in MATLAB. The ETD4RK method shows high efficiency and reliability among these methods for the NLSEs. The fourth order exponential time differencing Runge-Kutta (ETDRK4) time discretization we use in this paper is based on the ETD4RK method with a modification by Khaliq et al. in [24]. In [16], the ETDRK4 scheme has been applied to a single higher order nonlinear Schrödinger

(HONLS) equation. According to their numerical tests, the ETDRK4 is approximately four times faster than the fourth order split step Fourier method in simulating solutions of the HONLS equation. In [4, 17], Krylov subspace methods and Chebyshev approximations of the matrix exponential operator are introduced. The ETDRK4 method uses the same idea with these methods.

In this paper, we propose to apply LDG methods to solve the N-coupled NLSE (1.1). Based on different choice of numerical fluxes, we present both energy conserving and energy dissipative LDG methods. Experience reveals that energy conserving numerical methods, which conserve the discrete approximation of energy, are able to maintain the phase and shape of the waves accurately, especially for long time simulation [6, 9, 35]. We also provide an optimal error estimate for the proposed LDG-D method, and suboptimal error estimate for the LDG-C method applied to linear Schrödinger equation. Coupled with the efficient ETDRK4 time discretization, the proposed methods are very efficient and good for long-time computations as observed from our numerical experiments. A fourth order conservative time-stepping method [6] is also proposed. The efficiency of ETDRK4 and the conservative method is compared in the numerical experiments.

This paper is organized as follows. In Section 2, we start by providing a description of the LDG method for the NLSE, and showing its energy conservation and stability. Error estimate for the linear Schrödinger equation is then proven. In Section 3, we give an introduction to the ETDRK4 method for temporal discretization. The stability regions of the method are illustrated. In Section 4, A fourth order conservative time stepping method [6] is proposed. In Section 5, extensive numerical results of NLSEs are given showing convergence rates and efficiency of the methods. Several second order time stepping methods are also applied for an efficiency comparison. Finally, we give conclusion and future work in Section 6.

2 The local discontinuous Galerkin method

2.1 Notations

The computational domain $I=[a,b]$ is divided into N subintervals. We denote the cells by $I_j=[x_{j-1/2},x_{j+1/2}]$ for $j=1,\dots,N$. The center of the cell is $x_j=(x_{j-1/2}+x_{j+1/2})/2$ and the mesh size is $h_j=x_{j+1/2}-x_{j-1/2}$. We assume that the mesh is regular, namely, the ratio between the maximal and the minimal mesh sizes stays bounded during mesh refinement. The complex piecewise polynomial space V_h^k is defined as the space of polynomials of degree at most k in each cell I_j , that is

$$V_h^k = \{v: v \in P^k(I_j) \text{ for } x \in I_j, j=1, \dots, N\}.$$

Note that functions in V_h^k are allowed to have discontinuities across element interfaces, and are complex valued functions since the NLSE admits complex solutions.

We denote the numerical solution by u_h , which belongs to the finite element space V_h^k . $(u_h)_{j+1/2}^+$ and $(u_h)_{j+1/2}^-$ are the limit values of u_h at $x_{j+1/2}$ from the right cell I_{j+1}

and from the left cell I_j , respectively. We use the usual notations $[u_h] = u_h^+ - u_h^-$ and $\{u_h\} = (u_h^+ + u_h^-)/2$ to represent the jump and the average of the function u_h at the element interfaces. For any complex function w , its conjugate is denoted by w^* . The inner product of two functions w and r , and the L^2 norm of w over the interval I_j are given by

$$(w, r)_{I_j} = \int_{I_j} wr^* dx, \quad \|w\|_{I_j}^2 = \int_{I_j} ww^* dx = \int_{I_j} |w|^2 dx,$$

respectively.

2.2 The LDG method

In this subsection, we define the semi-discrete LDG method for the NLSE

$$iu_t + \epsilon u_{xx} + i(g(|u|^2)u)_x + f(|u|^2)u = 0, \quad (2.1)$$

with periodic boundary conditions and an initial condition

$$u(x, 0) = u_0(x). \quad (2.2)$$

Here $f(u)$ and $g(u)$ are arbitrary smooth nonlinear real functions. The periodic boundary condition is assumed for the sake of simplicity only and is not essential. The same method can be easily generalized for non-periodic boundary conditions. Also, we remark that the extension of the proposed LDG method to the N-coupled NLSE (1.1) is straightforward, as these equations are coupled through the last term $(\sum_{m=1}^N \beta_{nm} |u_m|^2)u_n$ only and that term does not include derivatives.

First, we introduce an auxiliary variable $q = u_x$, and write the wave equation into a first order system

$$\begin{aligned} iu_t + \epsilon q_x + i(g(|u|^2)u)_x + f(|u|^2)u &= 0, \\ q - u_x &= 0. \end{aligned} \quad (2.3)$$

The LDG method for (2.3) is then formulated as follows: find $u_h, q_h \in V_h^k$, such that

$$\begin{aligned} i((u_h)_t, v)_{I_j} - (\epsilon q_h, v_x)_{I_j} + \epsilon(\hat{q}_h(v^*)^-)_{j+\frac{1}{2}} - \epsilon(\hat{q}_h(v^*)^+)_{j-\frac{1}{2}} - i(g(|u_h|^2)u_h, v_x)_{I_j} \\ + i(\widehat{g}u_h(v^*)^-)_{j+\frac{1}{2}} - i(\widehat{g}u_h(v^*)^+)_{j-\frac{1}{2}} + (f(|u_h|^2)u_h, v)_{I_j} = 0, \end{aligned} \quad (2.4)$$

$$(q_h, w)_{I_j} + (u_h, w_x)_{I_j} - (\hat{u}_h(w^*)^-)_{j+\frac{1}{2}} + (\hat{u}_h(w^*)^+)_{j-\frac{1}{2}} = 0. \quad (2.5)$$

for all test functions $v, w \in V_h^k$. The hatted terms, \hat{q}_h , $\widehat{g}u_h$ and \hat{u}_h , in (2.4)-(2.5) are the cell boundary terms obtained from integration by parts, and they are the so-called numerical fluxes. These numerical fluxes are single-valued functions defined on the cell boundaries and should be designed according to guiding principles for different PDEs to ensure numerical stability. For the pair of \hat{q}_h and \hat{u}_h , we could use the simple alternating fluxes:

$$\hat{q}_h = q_h^-, \quad \hat{u}_h = u_h^+, \quad (2.6)$$

in which we have omitted the half-integer indices $j+1/2$, as all quantities in (2.6) are computed at the same points (i.e., the cell interface). We remark that the choice of the fluxes (2.6) is not unique. We can, for example, alternatively choose the numerical fluxes to be

$$\hat{q}_h = q_h^+, \quad \hat{u}_h = u_h^-. \quad (2.7)$$

For the other flux term $\widehat{g}u_h$, we could follow the approach in [36] and define

$$\widehat{g}u_h = \hat{g}(|u_h^-|^2, |u_h^+|^2)\tilde{u}_h, \quad (2.8)$$

where

$$\tilde{u}_h = \theta u_h^{up} + (1-\theta)\{u_h\}, \quad 0 < \theta \leq 1, \quad u_h^{up} = \begin{cases} u_h^- & \text{if } \hat{g} \geq 0, \\ u_h^+ & \text{if } \hat{g} < 0, \end{cases}$$

and $\hat{g}(a,b)$ is monotone flux, for example, the Lax-Friedrichs flux,

$$\hat{g}(a,b) = \frac{1}{2}(g(a) + g(b) - \gamma(b-a)), \quad \gamma = \max_l |g'(l)|.$$

The resulting scheme is denoted by LDG-D scheme. We could also define the flux $\widehat{g}u_h$ as

$$\widehat{g}u_h = \frac{\int_{|u_h^-|^2}^{|u_h^+|^2} g(s) ds}{[|u_h|^2]} \{u_h\} = \frac{[G(|u_h|^2)]}{[|u_h|^2]} \{u_h\}, \quad (2.9)$$

where

$$G(w) = \int^w g(s) ds. \quad (2.10)$$

The resulting scheme is called LDG-C scheme, where the 'C' and 'D' stand for conservative and dissipative, respectively, representing the energy-conserving and energy-dissipative property of the underlying schemes. For the N-coupled NLSE (1.1), the function $g(|u|^2)$ is chosen to be constant α_n , and the LDG-C scheme becomes a special case of LDG-D with $\theta=0$.

For simplicity, we introduce the notation

$$\mathcal{T}_j(r,s;\hat{r}) = - \int_{I_j} r s_x dx + (\hat{r} s^-)_{j+\frac{1}{2}} - (\hat{r} s^+)_{j-\frac{1}{2}}, \quad (2.11)$$

and the LDG methods (2.4)-(2.5) become

$$i((u_h)_t, v)_{I_j} + \epsilon \mathcal{T}_j(q_h, v^*; \hat{q}_h) + i \mathcal{T}_j(g(|u_h|^2) u_h, v^*; \widehat{g}u_h) + (f(|u_h|^2) u_h, v)_{I_j} = 0, \quad (2.12)$$

$$(q_h, w)_{I_j} = \mathcal{T}_j(u_h, w^*; \hat{u}_h). \quad (2.13)$$

One can easily observe that

$$\sum_j (\mathcal{T}_j(a,b;a^-) + \mathcal{T}_j(b,a;b^+)) = 0, \quad (2.14)$$

which will be utilized in our proof below.

2.3 Projections

We use P to denote the L^2 projection of a function $\omega(x)$ with $k+1$ continuous derivatives into space V_h^k , that is:

$$(P\omega, \phi)_\Omega = (\omega, \phi)_\Omega,$$

for any $\phi \in P^k$ on K .

In addition, a one-dimensional projection P^- for a real-valued function ω , which projects ω into the one-dimensional piecewise polynomial space of degree k while taking the values of ω at the cell interface, is defined as follows

$$(P^-\omega, \phi)_{I_j} = (\omega, \phi)_{I_j}, \quad \forall \phi \in P^{k-1}(I_j) \quad \text{and} \quad (P^-\omega)^-(x_{j+\frac{1}{2}}) = \omega^-(x_{j+\frac{1}{2}}). \quad (2.15)$$

Similarly, the one-dimensional projection $P^+\omega$ is defined as the projection of ω such that

$$(P^+\omega, \phi)_{I_j} = (\omega, \phi)_{I_j}, \quad \forall \phi \in P^{k-1}(I_j) \quad \text{and} \quad (P^+\omega)^+(x_{j-\frac{1}{2}}) = \omega^+(x_{j-\frac{1}{2}}).$$

For these projections, it is easy to show (see [10]):

$$\|\omega^e\| + h\|\omega^e\|_\infty + h^{\frac{1}{2}}\|\omega^e\|_{\Gamma_h} \leq Ch^{k+1}, \quad (2.16)$$

where $\omega^e = \omega - P\omega$ or $\omega^e = \omega - P^\pm\omega$, and Γ_h denotes the set of boundary points of all cells. The constant C depends on the function ω , but is independent of the mesh size h .

Let us now denote the errors for the function ω by

$$e_\omega = \omega - \omega_h, \quad \eta_\omega = \omega - P^\pm\omega, \quad \zeta_\omega = P^\pm\omega - \omega_h, \quad (2.17)$$

which, from left to right, respectively represent the errors between the exact solution and the numerical solution, the projection errors, and the errors between the numerical solution and the particular projection of the exact solution. Note that the signs of the projection P^\pm in (2.17) are consistent with the choice of the numerical fluxes in (2.6), and will be specified in the proposition below.

2.4 Energy conservation and stability

The L^2 stability of the LDG-D method, i.e. $\frac{d}{dt} \int |u_h|^2 dx \leq 0$, has been proved in [36]. In this subsection, we will show that the LDG-C method conserves the energy exactly, which will also give us its L^2 stability.

Proposition 2.1. The solution to the semi-discrete LDG-C method (2.4)-(2.5) with the choice of numerical fluxes (2.6)-(2.9) conserves the energy

$$E_h(t) = \|u_h\|_I^2 = \int_I |u_h|^2 dx \quad (2.18)$$

exactly for all time.

Proof. We first choose the test function $v = u_h$ in (2.4) and $w = \epsilon q_h$ in (2.5). The sum of these two equations gives

$$\begin{aligned} & i((u_h)_t, u_h)_{I_j} + \epsilon \mathcal{T}_j(q_h, u_h^*; q_h^-) + i \mathcal{T}_j(g(|u_h|^2)u_h, u_h^*; \widehat{g}u_h) \\ & + (f(|u_h|^2)u_h, u_h)_{I_j} + \epsilon(q_h, q_h)_{I_j} - \epsilon \mathcal{T}_j(u_h, q_h^*; u_h^+) = 0. \end{aligned} \quad (2.19)$$

We take the complex conjugate for every term in Eq. (2.19)

$$\begin{aligned} & -i((u_h^*)_t, u_h^*)_{I_j} + \epsilon \mathcal{T}_j(q_h^*, u_h; (q_h^*)^-) - i \mathcal{T}_j(g(|u_h|^2)u_h^*, u_h; \widehat{g}u_h^*) \\ & + (f(|u_h|^2)u_h^*, u_h^*)_{I_j} + \epsilon(q_h^*, q_h^*)_{I_j} - \epsilon \mathcal{T}_j(u_h^*, q_h; (u_h^*)^+) = 0. \end{aligned} \quad (2.20)$$

By subtracting Eqs. (2.19) and (2.20), summing up over all cells and using the periodic boundary conditions and (2.14), we have

$$i \frac{d}{dt} \|u_h\|_I^2 + i \sum_j \left(\mathcal{T}_j(g(|u_h|^2)u_h, u_h^*; \widehat{g}u_h) + \mathcal{T}_j(g(|u_h|^2)u_h^*, u_h; \widehat{g}u_h^*) \right) = 0.$$

Following the definition (2.9) of the flux $\widehat{g}u_h$, we have

$$\begin{aligned} & \sum_j \mathcal{T}_j(g(|u_h|^2)u_h, u_h^*; \widehat{g}u_h) + \sum_j \mathcal{T}_j(g(|u_h|^2)u_h^*, u_h; \widehat{g}u_h^*) \\ & = \sum_j \left[- \int_{I_j} g(|u_h|^2)u_h(u_h^*)_x dx + (\widehat{g}u_h(u_h^*)^-)_{j+\frac{1}{2}} - (\widehat{g}u_h(u_h^*)^+)_{j-\frac{1}{2}} \right. \\ & \quad \left. - \int_{I_j} g(|u_h|^2)u_h^*(u_h)_x dx + (\widehat{g}u_h^*(u_h)^-)_{j+\frac{1}{2}} - (\widehat{g}u_h^*(u_h)^+)_{j-\frac{1}{2}} \right] \\ & = - \sum_j \int_{I_j} g(|u_h|^2)(|u_h|^2)_x dx - \sum_j \frac{[G(|u_h|^2)]}{[|u_h|^2]} (\{u_h\}[u_h^*] + \{u_h^*\}[u_h]) \Big|_{j+\frac{1}{2}} \\ & = \sum_j [G(|u_h|^2)]_{j+\frac{1}{2}} - \sum_j [G(|u_h|^2)]_{j+\frac{1}{2}} = 0, \end{aligned}$$

where G is the antiderivative of g , as defined in (2.10). Therefore, we have

$$\frac{d}{dt} \|u_h\|_I^2 = 0.$$

and the quantity E_h is invariant in time. \square

Remark 2.1. The above energy conservation property is proven for the single NLSE. The same results hold for the N-coupled NLSE (1.1), which can be proven by similar techniques as that in the proof of Proposition 2.1, and hence the detailed proof is neglected here.

2.5 Error estimate

In this subsection, we carry out the error estimates for the linear Schrödinger equation, which takes the form of

$$iu_t + \epsilon u_{xx} + i(au)_x = 0. \quad (2.21)$$

Without loss of generality, we assume $\epsilon = a = 1$ to simplify our presentation. In [36], an error estimate of order $k+1/2$ has been shown for the LDG-D method with $\theta = 1$ in (2.8). Optimal error estimate for the equation without first order derivative term, i.e. $iu_t + u_{xx} = 0$, has recently been proven in [37] by Xu and Shu. Below, we will show that optimal error estimate can also be achieved for the LDG-D method with $\theta = 1$ applied to the equation (2.21) with a linear convection term. As we will show below, this extension is non-trivial and the presence of the first order derivative term adds many complexities to the proof. At the end of this subsection, we will show a suboptimal error estimate for the LDG-C method (i.e. $\theta = 0$ in (2.8)).

Let us first repeat the LDG-D method (2.12)-(2.13) here:

$$i((u_h)_t, v)_{I_j} + \mathcal{T}_j(q_h, v^*; \hat{q}_h) + i\mathcal{T}_j(u_h, v^*; \tilde{u}_h) = 0, \quad (2.22)$$

$$(q_h, w)_{I_j} = \mathcal{T}_j(u_h, w^*; \hat{u}_h), \quad (2.23)$$

with the numerical fluxes \hat{q}_h, \hat{u}_h defined in (2.6) or (2.7) and the upwind flux $\tilde{u}_h = u_h^-$. Note that if $a < 0$ in (2.21), the upwind flux \tilde{u}_h will become u_h^+ .

Since the proofs of the error estimate for different numerical fluxes are different, we start by presenting the following theorem when the numerical fluxes (2.7) are used:

Proposition 2.2. Let u , and q be the exact solutions of the linear Schrodinger equation (2.21), and let u_h , and q_h be the numerical solutions of the semi-discrete LDG method (2.22)-(2.23) with the numerical fluxes defined in (2.7) and the initial condition $u_h(\cdot, 0) = P^- u_0(x)$. The particular projections of the exact solutions are defined as $P^- u$, and $P^+ q$ in (2.17), and the corresponding errors are given by

$$\zeta_u = P^- u - u_h, \quad \zeta_q = P^+ q - q_h, \quad (2.24)$$

to be consistent with the choice of numerical fluxes. There holds the following error estimate:

$$\max_t \|e_u\|_I + \max_t \|e_q\|_I + \max_t \|(e_u)_t\|_I \leq Ch^{k+1}, \quad (2.25)$$

where $C = C(t, \|u\|_{L^\infty((0,t); H^{k+1}(I))}, \|u\|_{L^\infty((0,t); H^{k+2}(I))})$.

Proof. By the property of the projection (2.16), we can obtain the error estimates for the numerical initial conditions

$$\|e_u(x, 0)\|_I \leq Ch^{k+1}, \quad \|e_q(x, 0)\|_I \leq Ch^{k+1}, \quad \|(e_u)_t(x, 0)\|_I \leq Ch^{k+1}, \quad (2.26)$$

following the similar approach as in [8].

By subtracting the LDG method (2.22)-(2.23) with the fluxes (2.7) from the weak formulation satisfied by the exact solutions u , and q , we can derive the error equations

$$i((e_u)_t, v)_{I_j} + \mathcal{T}_j(e_q, v^*; e_q^+) + i\mathcal{T}_j(e_u, v^*; e_u^-) = 0, \quad (2.27)$$

$$(e_q, w)_{I_j} = \mathcal{T}_j(e_u, w^*; e_u^-), \quad (2.28)$$

for all test functions $v, w \in V_h^k$. By the definition of these projections P^\pm , we have

$$i((e_u)_t, v)_{I_j} + \mathcal{T}_j(\zeta_q, v^*; \zeta_q^+) + i\mathcal{T}_j(\zeta_u, v^*; \zeta_u^-) = 0, \quad (2.29)$$

$$(e_q, w)_{I_j} = \mathcal{T}_j(\zeta_u, w^*; \zeta_u^-). \quad (2.30)$$

Taking the test functions $v = \zeta_u$ and $w = \zeta_q$, and the sum of these two equations gives

$$i((e_u)_t, \zeta_u)_{I_j} + (e_q, \zeta_q)_{I_j} + \mathcal{T}_j(\zeta_q, \zeta_u^*; \zeta_q^+) + i\mathcal{T}_j(\zeta_u, \zeta_u^*; \zeta_u^-) = \mathcal{T}_j(\zeta_u, \zeta_q^*; \zeta_u^-). \quad (2.31)$$

We take the complex conjugate for every term in Eq. (2.31):

$$-i((e_u^*)_t, \zeta_u^*)_{I_j} + (e_q^*, \zeta_q^*)_{I_j} + \mathcal{T}_j(\zeta_q^*, \zeta_u; (\zeta_q^*)^+) - i\mathcal{T}_j(\zeta_u^*, \zeta_u; (\zeta_u^*)^-) = \mathcal{T}_j(\zeta_u^*, \zeta_q; (\zeta_u^*)^-). \quad (2.32)$$

By subtracting Eqs. (2.31) and (2.32), summing up over all cells and using the periodic boundary conditions and (2.14), we have

$$\begin{aligned} & i((e_u)_t, \zeta_u)_I + i(\zeta_u, (e_u)_t)_I + (e_q, \zeta_q)_I - (\zeta_q, e_q)_I \\ & \quad + i \sum_j (\mathcal{T}_j(\zeta_u, \zeta_u^*; \zeta_u^-) + \mathcal{T}_j(\zeta_u^*, \zeta_u; (\zeta_u^*)^-)) \\ = & i((e_u)_t, \zeta_u)_I + i(\zeta_u, (e_u)_t)_I + (e_q, \zeta_q)_I - (\zeta_q, e_q)_I + i \sum_j \|\zeta_u\|_{j+\frac{1}{2}}^2 = 0. \end{aligned} \quad (2.33)$$

By the decomposition of the error (2.17), and the properties of the projection error (2.16), we have

$$\begin{aligned} \frac{d}{dt} \|\zeta_u\|_I^2 & \leq -((\eta_u)_t, \zeta_u)_I - (\zeta_u, (\eta_u)_t)_I + i(\eta_q, \zeta_q)_I - i(\zeta_q, \eta_q)_I \\ & \leq Ch^{2k+2} + \frac{1}{3}(\|\zeta_q\|_I^2 + \|\zeta_u\|_I^2). \end{aligned} \quad (2.34)$$

which leads to

$$\|\zeta_u\|_I^2 \leq Ch^{2k+2} + \int_0^t \frac{1}{3}(\|\zeta_q\|_I^2 + \|\zeta_u\|_I^2) ds. \quad (2.35)$$

Next, we combine the error equations (2.29) and (2.30) to obtain

$$i((e_u)_t, v)_{I_j} + \mathcal{T}_j(\zeta_q, v^*; \zeta_q^+) + i(e_q, v)_{I_j} = 0. \quad (2.36)$$

We consider the time derivative of Eq. (2.30), and take the test functions $v = -(\zeta_u)_t$ in Eq. (2.36), $w = \zeta_q$ in Eq. (2.30). The sum of these two error equations gives

$$i((e_u)_t + e_q, -(\zeta_u)_t)_{I_j} + ((e_q)_t, \zeta_q)_{I_j} + \mathcal{T}_j(\zeta_q, -(\zeta_u)_t^*; \zeta_q^+) = \mathcal{T}_j((\zeta_u)_t, \zeta_q^*; (\zeta_u)_t^-). \quad (2.37)$$

By adding Eq. (2.37) and its complex conjugate, summing up over all cells and using the periodic boundary conditions and (2.14), we have

$$-i((e_u)_t + e_q, (\zeta_u)_t)_I + i((\zeta_u)_t, (e_u)_t + e_q)_I + ((e_q)_t, \zeta_q)_I + (\zeta_q, (e_q)_t)_I = 0. \quad (2.38)$$

By the decomposition of the error (2.17), and the properties of the projection error (2.16), we have

$$\begin{aligned} \frac{d}{dt} \|\zeta_q\|_I^2 &\leq i((\eta_u)_t + e_q, (\zeta_u)_t)_I - i((\zeta_u)_t, (\eta_u)_t + e_q)_I - ((\eta_q)_t, \zeta_q)_I - (\zeta_q, (\eta_q)_t)_I \\ &\leq Ch^{2k+2} + \frac{4}{3} (\|\zeta_q\|_I^2 + \|(\zeta_u)_t\|_I^2). \end{aligned} \quad (2.39)$$

which leads to

$$\|\zeta_q\|_I^2 \leq Ch^{2k+2} + \frac{4}{3} \int_0^t (\|\zeta_q\|_I^2 + \|(\zeta_u)_t\|_I^2) ds. \quad (2.40)$$

At the end, we consider the time derivative on both Eqs. (2.29)-(2.30), and take the test functions $v = (\zeta_u)_t$ and $w = (\zeta_q)_t$. The sum of these two equations gives

$$\begin{aligned} i((e_u)_{tt}, (\zeta_u)_t)_{I_j} + ((e_q)_t, (\zeta_q)_t)_{I_j} + \mathcal{T}_j((\zeta_q)_t, (\zeta_u)_t^*; (\zeta_q^+)_t) \\ + i\mathcal{T}_j((\zeta_u)_t, (\zeta_u)_t^*; (\zeta_u^-)_t) = \mathcal{T}_j((\zeta_u)_t, (\zeta_q^*)_t; (\zeta_u^-)_t). \end{aligned} \quad (2.41)$$

By subtracting Eq. (2.41) and its complex conjugate, summing up over all cells and using the periodic boundary conditions and (2.14), we have

$$\begin{aligned} i((e_u)_{tt}, (\zeta_u)_t)_I + i((\zeta_u)_t, (e_u)_{tt})_I + ((e_q)_t, (\zeta_q)_t)_I - ((\zeta_q)_t, (e_q)_t)_I \\ + i \sum_j (\mathcal{T}_j((\zeta_u)_t, (\zeta_u)_t^*; (\zeta_u^-)_t) + \mathcal{T}_j((\zeta_u)_t^*, (\zeta_u)_t; (\zeta_u^-)_t)) \\ = i((e_u)_{tt}, (\zeta_u)_t)_I + i((\zeta_u)_t, (e_u)_{tt})_I + ((e_q)_t, (\zeta_q)_t)_I - ((\zeta_q)_t, (e_q)_t)_I \\ + i \sum_j \|[(\zeta_u)_t]_{j+\frac{1}{2}}\|^2 \\ = 0. \end{aligned} \quad (2.42)$$

Hence, we have

$$\frac{d}{dt} \|(\zeta_u)_t\|_I^2 \leq -((\eta_u)_{tt}, (\zeta_u)_t)_I - ((\zeta_u)_t, (\eta_u)_{tt})_I + i((\eta_q)_t, (\zeta_q)_t)_I - i((\zeta_q)_t, (\eta_q)_t)_I. \quad (2.43)$$

We now integrate the equation (2.43) with respect to time between 0 and t . Applying integration by parts over t on each term, and the first term becomes

$$\int_0^t -((\eta_u)_{tt}, (\zeta_u)_t)_I dt = \int_0^t ((\eta_u)_{ttt}, \zeta_u)_I dt + ((\eta_u)_{tt}, \zeta_u)_I \Big|_0^t. \quad (2.44)$$

Combining (2.43), (2.44), and the properties of the projection error (2.16), we have

$$\|(\zeta_u)_t\|_I^2 \leq Ch^{2k+2} + \frac{1}{2}(\|\zeta_q\|_I^2 + \|\zeta_u\|_I^2) + \frac{1}{3} \int_0^t (\|\zeta_q\|_I^2 + \|\zeta_u\|_I^2) ds. \quad (2.45)$$

We now combine the three error inequalities (2.35), (2.40), and (2.45),

$$\begin{aligned} & \|\zeta_u\|_I^2 + \|\zeta_q\|_I^2 + \|(\zeta_u)_t\|_I^2 \\ & \leq Ch^{2k+2} + \frac{1}{2}(\|\zeta_q\|_I^2 + \|\zeta_u\|_I^2) + 2 \int_0^t (\|\zeta_q\|_I^2 + \|\zeta_u\|_I^2 + \|(\zeta_u)_t\|_I^2) ds. \end{aligned} \quad (2.46)$$

Applying the Gronwalls inequality, we obtain the optimal error estimate

$$\max_t \|\zeta_u\|_I^2 + \max_t \|\zeta_q\|_I^2 + \max_t \|(\zeta_u)_t\|_I^2 \leq Ch^{2k+2}. \quad (2.47)$$

□

We now consider the case when the other choice of numerical fluxes (2.6) is used in the LDG method. A new variable z , defined as $iu + q$, is introduced and used in the proof. Similarly, we have the numerical quantity $z_h = iu_h + q_h$.

Proposition 2.3. Let u , and q be the exact solutions of the linear Schrodinger equation (2.21), and let u_h , and q_h be the numerical solutions of the semi-discrete LDG method (2.22)-(2.23) with the numerical fluxes defined in (2.6) and the initial condition $u_h(\cdot, 0) = P^+ u_0(x)$. The particular projections of the exact solutions are defined as $P^+ u$, and $P^- z$ in (2.17), and the corresponding errors are given by

$$\zeta_u = P^+ u - u_h, \quad \zeta_z = P^+ z - z_h \quad (2.48)$$

to be consistent with the choice of numerical fluxes. There holds the following error estimate:

$$\max_t \|e_u(\cdot, t)\|_I + \max_t \|e_z(\cdot, t)\|_I \leq Ch^{k+1}, \quad (2.49)$$

where $C = C(t, \|u\|_{L^\infty((0,t); H^{k+1}(I))})$.

Proof. By the property of the projection (2.16), we obtain the error estimates for the numerical initial conditions

$$\|e_u(x, 0)\|_I \leq Ch^{k+1}, \quad \|e_z(x, 0)\|_I \leq Ch^{k+1}, \quad (2.50)$$

following the similar approach as in [8].

By subtracting the LDG method (2.22)-(2.23) with the fluxes (2.7) from the weak formulation satisfied by the exact solutions u , and z , and using the properties of the projections P_h^\pm , we can derive the error equations

$$i((e_u)_t, v)_{I_j} + \mathcal{T}_j(\zeta_z, v^*; \zeta_z^-) = 0, \quad (2.51)$$

$$(e_z - ie_u, w)_{I_j} = \mathcal{T}_j(\zeta_u, w^*; \zeta_u^+), \quad (2.52)$$

for all test functions $v, w \in V_h^k$. Taking the test functions $v = \zeta_u$ and $w = \zeta_z$, and the sum of these two equations gives

$$i((e_u)_t, \zeta_u)_{I_j} + (e_z - ie_u, \zeta_z)_{I_j} + \mathcal{T}_j(\zeta_z, \zeta_u^*; \zeta_z^-) = \mathcal{T}_j(\zeta_u, \zeta_z^*; \zeta_u^+). \quad (2.53)$$

By subtracting Eq.(2.53) and its complex conjugate, summing up over all cells and using the periodic boundary conditions and (2.14), we have

$$i((e_u)_t, \zeta_u)_I + i(\zeta_u, (e_u)_t)_I + (e_z - ie_u, \zeta_z)_I - (\zeta_z, e_z - ie_u)_I = 0. \quad (2.54)$$

By the decomposition of the error (2.17), and the properties of the projection error (2.16), we have

$$\begin{aligned} \frac{d}{dt} \|\zeta_u\|_I^2 &\leq -((\eta_u)_t, \zeta_u)_I - (\zeta_u, (\eta_u)_t)_I + i(\eta_z, \zeta_q)_I - i(\zeta_q, \eta_z)_I - i(ie_u, \zeta_q)_I + i(\zeta_q, ie_u)_I \\ &\leq Ch^{2k+2} + \frac{3}{2}(\|\zeta_z\|_I^2 + \|\zeta_u\|_I^2), \end{aligned} \quad (2.55)$$

which leads to

$$\|\zeta_u\|_I^2 \leq Ch^{2k+2} + \int_0^t \frac{3}{2}(\|\zeta_q\|_I^2 + \|\zeta_u\|_I^2) ds. \quad (2.56)$$

Next, we consider the time derivative of Eq. (2.52), and take the test functions $v = -(\zeta_u)_t + \zeta_z$ in Eq. (2.51) and $w = \zeta_z$ in Eq. (2.52). The sum of these two error equations gives

$$\begin{aligned} i((e_u)_t, -(\zeta_u)_t + \zeta_z)_{I_j} + ((e_z - ie_u)_t, \zeta_z)_{I_j} + \mathcal{T}_j(\zeta_z, -(\zeta_u)_t^* + \zeta_z^*; \zeta_z^-) \\ = \mathcal{T}_j((\zeta_u)_t, \zeta_z^*; (\zeta_u)_t^+). \end{aligned} \quad (2.57)$$

By adding Eq. (2.57) and its complex conjugate, summing up over all cells and using the periodic boundary conditions and (2.14), we have

$$\begin{aligned} i((e_u)_t, -(\zeta_u)_t + \zeta_z)_I - i(-(\zeta_u)_t + \zeta_z, (e_u)_t)_I + ((e_z - ie_u)_t, \zeta_z)_I \\ + (\zeta_z, (e_z - ie_u)_t)_I + \sum_j (\mathcal{T}_j(\zeta_z, \zeta_z^*; \zeta_z^-) + \mathcal{T}_j(\zeta_z^*, \zeta_z; (\zeta_z^-)^*)) \\ = i((e_u)_t, -(\zeta_u)_t + \zeta_z)_I - i(-(\zeta_u)_t + \zeta_z, (e_u)_t)_I + ((e_z - ie_u)_t, \zeta_z)_I \\ + (\zeta_z, (e_z - ie_u)_t)_I + \sum_j \|\zeta_z\|_{j+\frac{1}{2}}^2 = 0. \end{aligned} \quad (2.58)$$

By the decomposition of the error (2.17), and the properties of the projection error (2.16), we have

$$\frac{d}{dt} \|\zeta_z\|_I^2 \leq i((\eta_u)_t, (\zeta_u)_t)_I - i((\zeta_u)_t, (\eta_u)_t)_I - ((\eta_z)_t, \zeta_z)_I - (\zeta_z, (\eta_z)_t)_I. \quad (2.59)$$

We now integrate the equation (2.59) with respect to time between 0 and t . Applying integration by parts over t on the first two terms, and the first term becomes

$$\int_0^t ((\eta_u)_t, (\zeta_u)_t)_I dt = \int_0^t ((\eta_u)_{tt}, \zeta_u)_I dt + ((\eta_u)_{tt}, \zeta_u)_I|_0^t. \quad (2.60)$$

Combining (2.59), (2.60), and the properties of the projection error (2.16), we have

$$\|\zeta_z\|_I^2 \leq Ch^{2k+2} + \frac{1}{2}(\|\zeta_u\|_I^2) + \frac{1}{2} \int_0^t (\|\zeta_z\|_I^2 + \|\zeta_u\|_I^2) ds. \quad (2.61)$$

We now combine the two error inequalities (2.56), and (2.61),

$$\|\zeta_u\|_I^2 + \|\zeta_z\|_I^2 \leq Ch^{2k+2} + \frac{1}{2}(\|\zeta_u\|_I^2) + 2 \int_0^t (\|\zeta_z\|_I^2 + \|\zeta_u\|_I^2) ds. \quad (2.62)$$

Applying the Gronwalls inequality, we obtain the error estimate

$$\max_t \|\zeta_u\|_I^2 + \max_t \|\zeta_z\|_I^2 \leq Ch^{2k+2}. \quad (2.63)$$

□

Next, we would like to provide an error estimate for the LDG-C method. If $\epsilon = 0$ in the linear Schrödinger equation (2.1), the equation becomes the simple linear transport equation $u_t + (au)_x = 0$, and it is well-known that we can only prove suboptimal error estimate for the DG method with a central flux (i.e., the LDG-C method with $\epsilon = 0$). We would expect the same result here, and provide a suboptimal error estimate for the LDG-C method below.

Let us repeat the LDG-C method (2.12)-(2.13) here:

$$i((u_h)_t, v)_{I_j} + \mathcal{T}_j(q_h, v^*; \hat{q}_h) + i\mathcal{T}_j(u_h, v^*; \tilde{u}_h) = 0, \quad (2.64)$$

$$(q_h, w)_{I_j} = \mathcal{T}_j(u_h, w^*; \hat{u}_h), \quad (2.65)$$

with the numerical fluxes \hat{q}_h, \hat{u}_h defined in (2.6) or (2.7) and the central flux $\tilde{u}_h = \{u_h\}$. For both choices of the numerical fluxes \hat{q}_h, \hat{u}_h , we have the following theorem:

Proposition 2.4. Let u , and q be the exact solutions of the linear Schrodinger equation (2.21), and let u_h , and q_h be the numerical solutions of the semi-discrete LDG-D method (2.64)-(2.65). The particular projections of the exact solutions are defined as $P^\pm u$ to be consistent with the choice of numerical flux \hat{u}_h , and Pq . There holds the following error estimate:

$$\|e_u\|_I \leq Ch^k, \quad (2.66)$$

where $C = C(t, \|u\|_{L^\infty((0,t); H^{k+1}(I))})$.

Proof. Without loss of generality, we assume the numerical flux (2.6) is used.

By subtracting the LDG method (2.64)-(2.65) from the weak formulation satisfied by the exact solutions u , and q , and the definition of the projections P^+u , we can derive the error equations

$$i((e_u)_t, v)_{I_j} + \mathcal{T}_j(e_q, v^*; e_q^-) + i\mathcal{T}_j(e_u, v^*; \{e_u\}) = 0, \quad (2.67)$$

$$(e_q, w)_{I_j} = \mathcal{T}_j(\zeta_u, w^*; \zeta_u^+), \quad (2.68)$$

for all test functions $v, w \in V_h^k$. Taking the test functions $v = \zeta_u$ and $w = \zeta_q$, and the sum of these two equations gives

$$i((e_u)_t, \zeta_u)_{I_j} + (e_q, \zeta_q)_{I_j} + \mathcal{T}_j(e_q, \zeta_u^*; e_q^-) + i\mathcal{T}_j(e_u, \zeta_u^*; \{e_u\}) = \mathcal{T}_j(\zeta_u, \zeta_q^*; \zeta_u^+). \quad (2.69)$$

By subtracting Eqs. (2.69) and its complex conjugate, summing up over all cells, using the periodic boundary conditions, the definition of the projection Pq and (2.14), we have

$$\begin{aligned} & i((e_u)_t, \zeta_u)_I + i(\zeta_u, (e_u)_t)_I + (e_q, \zeta_q)_I - (\zeta_q, e_q)_I + i \sum_j (\mathcal{T}_j(e_u, \zeta_u^*; \{e_u\}) + \mathcal{T}_j(e_u^*, \zeta_u; \{e_u^*\})) \\ & + \sum_j \left(\mathcal{T}_j(e_q, \zeta_u^*; e_q^-) - \mathcal{T}_j(e_q^*, \zeta_u; (e_q^-)^*) - \mathcal{T}_j(\zeta_u, \zeta_q^*; \zeta_u^+) + \mathcal{T}_j(\zeta_u^*, \zeta_q; (\zeta_u^+)^*) \right) \\ & = i((e_u)_t, \zeta_u)_I + i(\zeta_u, (e_u)_t)_I - \sum_j \left(i\{\eta_u\}[\zeta_u^*] + i\{\eta_u^*\}[\zeta_u] + \eta_q^-[\zeta_u^*] - (\eta_q^-)^*[\zeta_u] \right)_{j+\frac{1}{2}} \\ & = i((e_u)_t, \zeta_u)_I + i(\zeta_u, (e_u)_t)_I - \sum_j \left(\frac{i}{2}\eta_u^-[\zeta_u^*] + \frac{i}{2}(\eta_u^-)^*[\zeta_u] + \eta_q^-[\zeta_u^*] - (\eta_q^-)^*[\zeta_u] \right)_{j+\frac{1}{2}} = 0. \end{aligned} \quad (2.70)$$

By the decomposition of the error (2.17), and the properties of the projection error (2.16), we have

$$\begin{aligned} \frac{d}{dt} \|\zeta_u\|_I^2 & \leq -((\eta_u)_t, \zeta_u)_I - (\zeta_u, (\eta_u)_t)_I + \sum_j \left(\frac{1}{2}\eta_u^-[\zeta_u^*] + \frac{1}{2}(\eta_u^-)^*[\zeta_u] - i\eta_q^-[\zeta_u^*] + i(\eta_q^-)^*[\zeta_u] \right)_{j+\frac{1}{2}} \\ & \leq Ch^{2k+2} + \frac{1}{2}\|\zeta_u\|_I^2 + C_1 \sum_j h^{-1} \left(|\eta_u^- / 2|_{j+\frac{1}{2}} + |\eta_q^-|_{j+\frac{1}{2}} \right)^2 + \frac{1}{2C_2} \sum_j h \|\zeta_u\|_{j+\frac{1}{2}}^2 \\ & \leq Ch^{2k+2} + Ch^{2k} + \|\zeta_u\|_I^2. \end{aligned} \quad (2.71)$$

which leads to

$$\|\zeta_u\|_I^2 \leq Ch^{2k}. \quad (2.72)$$

Combined with the projection error (2.16), we can derive the suboptimal error estimate (2.66). \square

Remark 2.2. In this subsection, we only consider the LDG-C method with $\theta = 0$ in the flux (2.8), and the LDG-D method with $\theta = 1$. For the more general case when $0 < \theta < 1$, it is straightforward to apply the proof of Proposition 2.4 and obtain a suboptimal error estimate. In order to provide an optimal error estimate (which we expect), a global projection is needed to eliminate the boundary term coming from this flux. In a recent paper by Meng et. al. [27], such projection is constructed and optimal error estimate is provided for the simple linear equation $u_t + u_x = 0$. For our problem, the error estimate is much more complicated due to the second order derivative term, and we will leave this for future investigation.

3 Fourth order exponential time differencing Runge-Kutta method

For a single NLSE like equation (2.1), the energy of the numerical solution $E(u)$ is denoted by $\int_{-\infty}^{\infty} |u|^2 dx$, which can be conveniently evaluated via the spectral norm $\|u\|_2$. In Subsection 2.1, we prove that the proposed semi-discrete LDG-C method conserves the energy exactly. In [30], five different time discretizations are applied to the single NLSE. They have done extensively numerical investigation and three of them (one explicit RK2 scheme and two splitting methods) have been found to perform poorly and have nonlinear blow-up in finite time. A detailed study of the nonlinear blow-up was carried out in [30], and it can be linked back to the energy increasing of the underlying time discretization. In this paper, we will utilize the efficient ETDRK4 method as our time discretization, and can numerically observe that its energy does not increase in time.

3.1 The ETDRK4 method

The ETDRK4 method was constructed to solve the equation of the form

$$u_t = \mathcal{L}u + \mathcal{F}(u, t), \quad (3.1)$$

where \mathcal{L} is a linear operator and \mathcal{F} is nonlinear. After being discretized in space, equation (3.1) can be written as a system of ODEs of the form

$$u_t + Au = F(u, t). \quad (3.2)$$

Considering the LDG method applied to N-coupled NLSE (1.1), the semi-discrete method can be rewritten as

$$\begin{aligned} \mathbf{M} \frac{dU}{dt} + \mathbf{S}U &= \mathbf{F}(U) \\ \Rightarrow \frac{dU}{dt} + \mathbf{M}^{-1}\mathbf{S}U &= \mathbf{M}^{-1}\mathbf{F}(U), \end{aligned} \quad (3.3)$$

which is in the form of (3.2). Here \mathbf{M} is the mass matrix, \mathbf{S} is the stiffness matrix approximating the linear term $i\alpha_n u_{nx} + \epsilon_n u_{nxx}$, \mathbf{F} approximates the nonlinear term $(\sum_{m=1}^N \beta_{mn} |u_n|^2) u_n$, and U is a vector containing the coefficients of the solution u_n on the polynomial basis.

We integrate equation (3.2) over a single time step from $t = t_n$ to $t_{n+1} = t_n + \Delta t$ and get

$$u(t^{n+1}) = e^{-\tau A} u(t^n) + e^{-\tau A} \int_0^\tau e^{tA} F(u(t^n+t), t^n+t) dt. \quad (3.4)$$

To be consistent with the notations in Subsection 2.1, we denote the numerical approximation of $u(t_n)$ by u_h^n and denote $F(u_h^n, t^n)$ by F_h^n . The time step Δt is set as τ .

Different exponential time differencing (ETD) time discretization is obtained based on the formulation (3.4). For example, the first order ETD takes the form of

$$u_h^{n+1} = e^{-\tau A} u_h^n + A^{-1} (I - e^{-\tau A}) F_h^n. \quad (3.5)$$

Several different ETD approximations are listed in [38], here we consider the fourth-order ETD scheme introduced in [14, 22]. In [24], the scheme was modified so that the resulting ETDRK4 scheme does not require computation of higher powers of the matrix inverse. As explained in [24], the term e^{-z} is approximated by the fourth-order (2, 2)-Padé scheme and the ETDRK4 comes as

$$\begin{aligned} u_h^{n+1} &= R_{2,2}(\tau A) u_h^n + P_1(\tau A) F(u_h^n, t_n) \\ &\quad + P_2(\tau A) \left(F(a^n, t_n + \tau/2) + F(b^n, t_n + \tau/2) \right) + P_3(\tau A) F(c^n, t_n + \tau), \end{aligned} \quad (3.6)$$

where

$$\begin{aligned} R_{2,2}(\tau A) &= (12I - 6\tau A + \tau^2 A^2)(12I + 6\tau A + \tau^2 A^2)^{-1}, \\ P_1(\tau A) &= \tau(2I - \tau A)(12I + 6\tau A + \tau^2 A^2)^{-1}, \\ P_2(\tau A) &= 4\tau(12I + 6\tau A + \tau^2 A^2)^{-1}, \\ P_3(\tau A) &= \tau(2I + \tau A)(12I + 6\tau A + \tau^2 A^2)^{-1}, \\ a^n &= R_{2,2}(\tau A/2) u_h^n + P(\tau A) F(u_h^n, t_n), \\ b^n &= R_{2,2}(\tau A/2) u_h^n + P(\tau A) F(a^n, t_n + \tau/2), \\ c^n &= R_{2,2}(\tau A/2) a^n + P(\tau A) \left(2F(b^n, t_n + \tau/2) - F(u_h^n, t_n) \right), \\ P(\tau A) &= 24\tau(48I + 12\tau A + \tau^2 A^2)^{-1}. \end{aligned}$$

We notice that in this scheme, the matrix inverses we need are $(12I + 6\tau A + \tau^2 A^2)^{-1}$ and $(48I + 12\tau A + \tau^2 A^2)^{-1}$. So we can compute and store them during the initialization process to save computational time. To avoid computational inaccuracies due to high condition numbers and roundoff error in computing the power of the matrices, a partial fraction decomposition is used for scheme (3.6), as explained in [24]. The partial fractions in the decomposition involve complex shifts of the operator A . These complex shifts come in conjugate pairs and correspond to complex poles of the rational function under consideration, which are the roots of the real denominators. Therefore, the ETDRK4 scheme is modified to the following four steps, where $\Re(z)$ denotes the real part of z :

1. a^n is updated by

$$a^n = u_n + 2\Re(\alpha),$$

where α is the solution of

$$(\tau A - \tilde{c}_1 I)\alpha = \tilde{w}_1 u_h^n + \tau \tilde{\Omega}_1 F(u_h^n, t_n).$$

2. b^n is updated by

$$b^n = u_n + 2\mathfrak{R}(\beta),$$

where β is the solution of

$$(\tau A - \tilde{c}_1 I)\beta = \tilde{w}_1 u_h^n + \tau \tilde{\Omega}_1 F(a^n, t_n + \tau/2).$$

3. c^n is updated by

$$c^n = a_h^n + 2\mathfrak{R}(\gamma),$$

where γ is the solution of

$$(\tau A - \tilde{c}_1 I)\gamma = \tilde{w}_1 a^n + \tau \tilde{\Omega}_1 (2F(b^n, t_n + \tau/2) - F(u_h^n, t_n)).$$

4. u_h^{n+1} is updated by

$$u_h^{n+1} = u_h^n + 2\mathfrak{R}(\phi),$$

where ϕ is the solution of

$$(\tau A - c_1 I)\phi = w_1 u_n + \tau w_{11} F(u_h^n, t_n) + \tau w_{21} (F(a^n, t_n + \tau/2) + F(b^n, t_n + \tau/2)) + \tau w_{31} F(c^n, t_n + \tau).$$

Here, w and c are the coefficients used for the weights and poles:

$$\begin{aligned} c_1 &= -3.0 + i1.73205080756887729352, \\ w_1 &= -6.0 - i10.3923048454132637611, \\ w_{11} &= -0.5 - i1.44337567297406441127, \\ w_{21} &= -i1.15470053837925152901, \\ w_{31} &= 0.5 + i0.28867513459481288225, \\ \tilde{c}_1 &= -6.0 + i3.4641016151377545870548, \\ \tilde{w}_1 &= -12.0 - i20.78460969082652752232935, \\ \tilde{\Omega}_1 &= -i3.46410161513775458705. \end{aligned}$$

3.2 Stability regions

The stability of the ETDRK4 can be analyzed by plotting its stability regions (see also [14] and [18]). Consider the nonlinear ODE

$$u_t = cu + F(u), \tag{3.7}$$

where $F(u)$ is the nonlinear part, we suppose there exists a fixed point u_0 such that $cu_0 + F(u_0) = 0$. If u is the perturbation of u_0 and $\lambda = F'(u_0)$, then after linearizing, we have

$$u_t = cu + \lambda u. \tag{3.8}$$

The fixed point u_0 is stable if $Re(c+\lambda) < 0$. Denote $x = \lambda\tau$ and $y = c\tau$, where τ is the time step and apply the ETDRK4 method to (3.8), then we can compute the amplification factor:

$$\frac{u_{n+1}}{u_n} = r(x, y) = c_0 + c_1x + c_2x^2 + c_3x^3 + c_4x^4, \quad (3.9)$$

where

$$\begin{aligned} c_0 &= \frac{1327104 - 331776y - 55296y^2 + 20736y^3 + 3456y^4 - 2160y^5 + 372y^6 - 30y^7 + y^8}{(48 - 12y + y^2)^3(12 - 6y + y^2)} \\ c_1 &= \frac{1327104 - 331776y - 55296y^2 + 20736y^3 - 3456y^4 + 432y^5 - 36y^6}{(48 - 12y + y^2)^3(12 - 6y + y^2)} \\ c_2 &= \frac{663552 - 165888y - 27648y^2 + 8064y^3 - 288y^4 - 48y^5}{(48 - 12y + y^2)^3(12 - 6y + y^2)} \\ c_3 &= \frac{221184 - 55296y - 9216y^2 - 1152y^3}{(48 - 12y + y^2)^3(12 - 6y + y^2)} \\ c_4 &= \frac{55296 - 27648y}{(48 - 12y + y^2)^3(12 - 6y + y^2)}. \end{aligned}$$

We notice that when $y=0$, the amplification factor (3.9) becomes

$$r(x,0) = 1 + x + \frac{1}{2}x^2 + \frac{1}{6}x^3 + \frac{1}{24}x^4,$$

which is the amplification factor for the explicit fourth-order Runge-Kutta (RK4) method. The stability regions are shown in Fig. 1, where we plot the real and imaginary part of x with fixed y as real values $0, -5, -10, -20$.

4 Energy conserving time-stepping method

In section 2, we have proposed both energy conserving (LDG-C) and energy dissipative (LDG-D) methods for the Schrödinger equation. In order to extend the energy conservation property of the the semi-discrete LDG-C method to the fully discrete method, it is natural to employ time stepping methods which also conserve discrete energy. A family of temporal integrators having arbitrarily high order in time and which does preserve the conservation laws up to round-off error is the implicit Runge-Kutta collocation type methods associated with the diagonal elements of the Padé table for e^z . In this section, we consider the first two members of this family of energy conserving schemes.

For the NLSE taking the form of

$$iu_t + \epsilon u_{xx} + i(au)_x + f(|u|^2)u = 0, \quad (4.1)$$

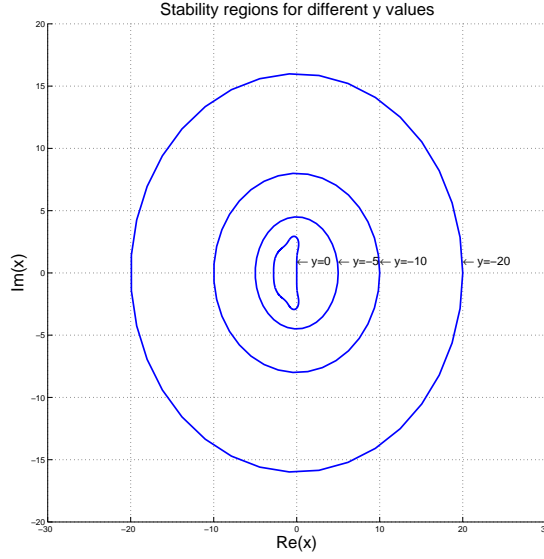


Figure 1: Stability regions of the ETD4 with y fixed to some negative values.

the fully discrete second-order in time LDG-C approximations are constructed using the *midpoint rule* in the following manner:

$$i \left(\frac{u_h^{n+1} - u_h^n}{\tau}, v \right)_{I_j} + \epsilon \mathcal{T}_j \left(\frac{q_h^{n+1} + q_h^n}{2}, v^*; \frac{\hat{q}_h^{n+1} + \hat{q}_h^n}{2} \right) + i \mathcal{T}_j \left(a \frac{u_h^{n+1} + u_h^n}{2}, v^*; \frac{a \hat{u}_h^{n+1} + a \hat{u}_h^n}{2} \right) + \left(\widetilde{f(|u_h|^2)} \frac{u_h^{n+1} + u_h^n}{2}, v \right)_{I_j} = 0, \quad (4.2)$$

$$(q_h^n, w)_{I_j} = \mathcal{T}_j(u_h^n, w^*; \hat{u}_h^n), \quad (4.3)$$

$$(q_h^{n+1}, w)_{I_j} = \mathcal{T}_j(u_h^{n+1}, w^*; \hat{u}_h^{n+1}). \quad (4.4)$$

for all test functions $v, w \in V_h^k$, where

$$\widetilde{f(|u_h|^2)} = \frac{F(|u^{n+1}|^2) - F(|u^n|^2)}{|u^{n+1}|^2 - |u^n|^2},$$

with $F(a) = \int^a f(s) ds$.

By taking $v = (u_h^{n+1} + u_h^n)/2$, $w = (q_h^{n+1} + q_h^n)/2$ in (4.2)-(4.4) and some simple algebra, we can derive that $\|u_h^{n+1}\|_I^2 = \|u_h^n\|_I^2$, which is the discrete energy conservation property. Even more, for the case when $a=0$, the NLSE equation conserves the term $\|q\|_I^2 + F(|u|^2)$,

in addition to the energy $\|u\|^2$. We can also prove that the above energy conserving method in (4.2)-(4.4) conserve the term $\|q^n\|_I^2 + F(|u_h^n|^2)$ in the discrete level as well.

A fourth order energy conserving time-stepping method based on the midpoint rule is provided in [6] to solve nonlinear system (3.2). Let $u^{n+1} \in V_h^k$ be defined as

$$u^{n+1} = u^n + \sqrt{3}(u^{n,2} - u^{n,1}), \quad (4.5)$$

with $u^{n,1}$ and $u^{n,2}$ given as solutions of the coupled system of equations,

$$\begin{aligned} u^{n,1} - u^n + \tau(a_{11}f^{n,1} + a_{12}f^{n,2}) &= 0, \\ u^{n,2} - u^n + \tau(a_{21}f^{n,1} + a_{22}f^{n,2}) &= 0, \end{aligned}$$

where $f^{n,i} = Au^{n,i} - F(u^{n,i}, t)$, $i=1,2$ and $a_{11}=a_{22}=1/4$, $a_{12}=1/4 - \sqrt{3}/6$, $a_{21}=1/4 + \sqrt{3}/6$.

5 Numerical results

In this section we present numerical results of our ETDRK4 LDG methods for the one-dimensional single and N-coupled NLSEs. We implemented the fourth order finite element LDG method (i.e. $k=3$), coupled with the fourth order ETDRK4 time discretization. Both the energy conserving LDG-C and energy dissipative LDG-D methods will be tested. In the implementation, we decompose the complex function $u(x,t)$ into the real and imaginary parts, and involve them in time.

5.1 Single NLSE

We consider the single NLSE

$$iu_t + u_{xx} + i\alpha(|u|^2u)_x + \beta|u|^2u + \gamma|u|^4u = 0, \quad (5.1)$$

which admits an exact solution

$$u(x,t) = A \exp(i(cx - \omega t)), \quad (5.2)$$

where $\omega = c^2 + \alpha|A|^2c - \beta|A|^2 - \gamma|A|^4$. In this numerical test, we set $\alpha = 0.5, \beta = \gamma = 1, A = c = 1$, with periodic boundary condition in $[0, 2\pi]$.

The surface plots of the real and imaginary parts of the results by the ETDRK4 using LDG-C are shown in Fig. 2. We utilize different temporal steps τ and compare the results with the exact solution at $t = 1$ to have Fig. 3 which indicates the convergence rate of ETDRK4. The slopes of the regression line for errors of both real and imaginary parts are close to 4 which corresponds to the fourth order method in time. It can be seen from Fig. 4 and Fig. 5 that both LDG-C and LDG-D methods demonstrate a fourth order accuracy in space.

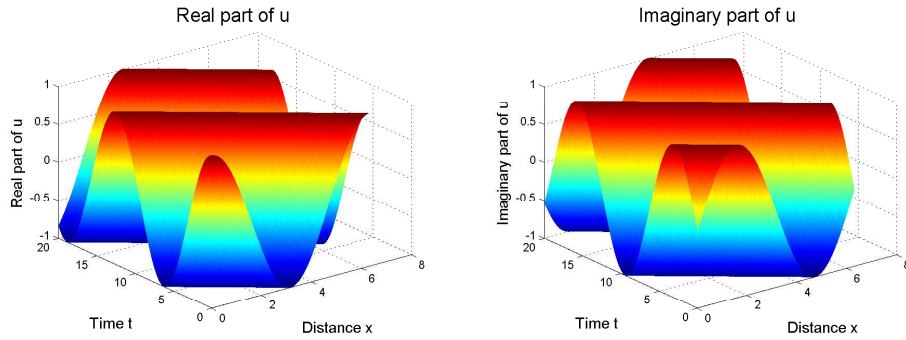


Figure 2: Surface plots of the results by the ETDRK4 solving single NLSE (5.1) using LDG-C in space ($N=128$, $\tau=0.1$ and $T=[0, 20]$).

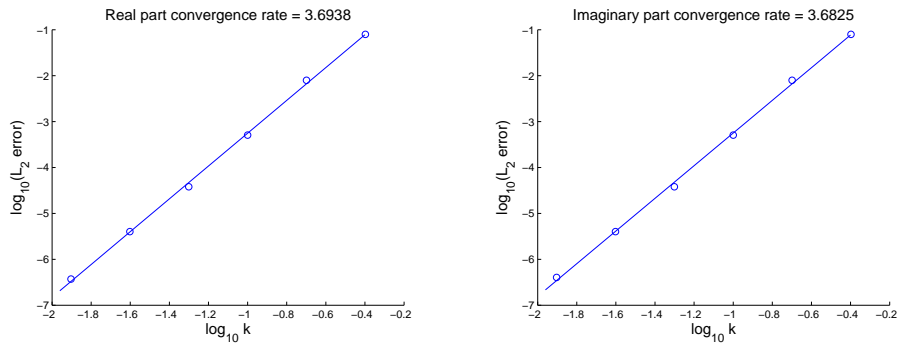


Figure 3: Convergence rate of results by the ETDRK4 solving single NLSE (5.1) using LDG-C in space ($N=128$).

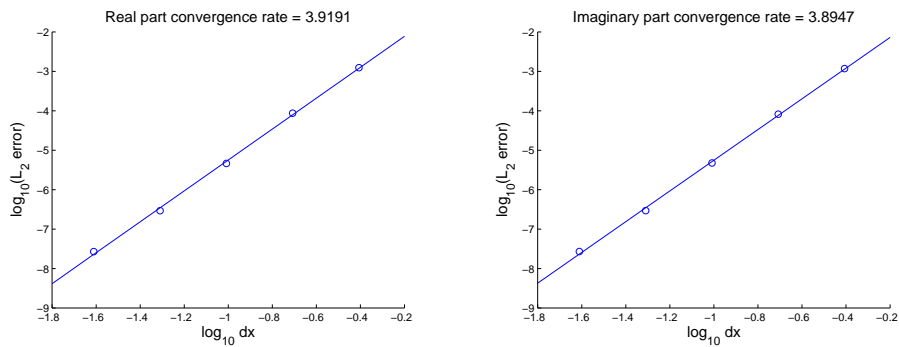


Figure 4: Convergence rate of results by LDG-C solving single NLSE (5.1) using ETDRK4 in time ($\tau=0.01$).

Fig. 6 contains the time history of the energy of results by the ETDRK4 and the Fourth-

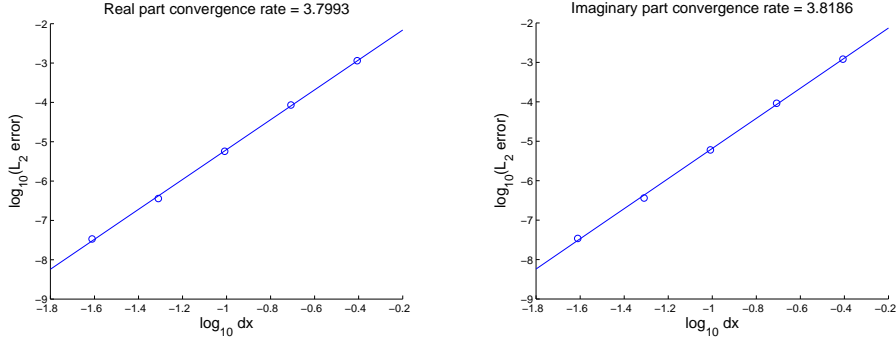


Figure 5: Convergence rate of results by LDG-D solving single NLSE (5.1) using ETDRK4 in time ($\tau=0.01$).

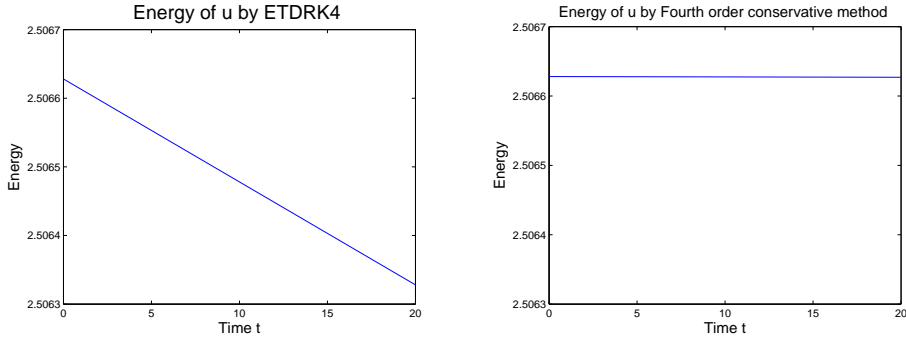


Figure 6: Comparison of energy changes of results by the ETDRK4 ($\tau=0.1$) and the Fourth-order conservative method (4.5) ($\tau=0.1$) solving single NLSE (5.1) using LDG-C in space ($N=128$).

order conservative method (4.5) with the same spatial discretization. We notice that the result by the ETDRK4 has energy that decreases slightly as time increases and the result by the Fourth-order conservative method (4.5) conserves the energy exactly but it requires an iterative nonlinear solver such as the Newton's method [19]. We will compare the efficiency of these two temporal methods in the following discussion.

To observe the behavior on energy conservation of LDG-C and LDG-D methods, we use the Fourth-order conservative method (4.5) in time and record the change of energy in Fig. 7. It can be noticed that the LDG-C method conserves energy exactly while the LDG-D method is dissipative. In the LDG-D method, θ is chosen to be 1.

Table 1 indicates the CPU time and L_2 errors of Crank-Nicolson method [19], Second-order conservative method [6] and the ETD-CN method [26] on (5.1). These are second-order methods in time. The first two methods conserve the energy exactly but they require an iterative nonlinear solver such as the Newton's method [19]. The ETD-CN method achieves a higher efficiency considering the CPU time and accuracy with a little

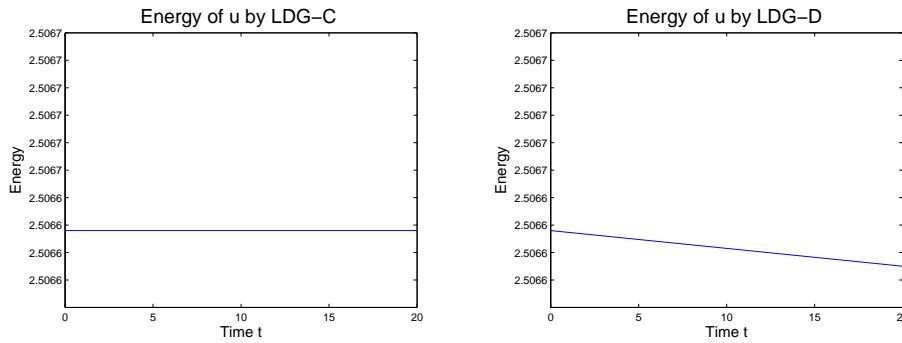


Figure 7: Comparison of energy changes of results by LDG-C in space ($N=128$) and LDG-D in space ($N=128$) solving single NLSE (5.1) using Fourth-order conservative method (4.5) in time ($\tau=0.1$).

Table 1: A comparison of efficiencies of Crank-Nicolson method [19], the Second-order conservative method [6] and the ETD-CN method [26] using LDG-C ($N=128$) on (5.1) (the time step is chosen to be $\tau=0.01$).

T	Crank-Nicolson			Second-order conservative			ETD-CN		
	CPUtime	L_2 error	energy	CPUtime	L_2 error	energy	CPUtime	L_2 error	energy
5	5.57e+2	0.00157	2.506628	6.12e+2	0.00125	2.506628	2.5206	6.1342e-5	2.506628
10	9.36e+2	0.00315	2.506628	1.02e+3	0.00251	2.506628	4.2736	1.2268e-4	2.506731
20	1.78e+3	0.00630	2.506628	1.93e+3	0.00503	2.506628	7.4643	2.4536e-4	2.506937
30	2.61e+3	0.00946	2.506628	2.91e+3	0.00754	2.506628	10.6532	4.9072e-4	2.507143

sacrifice in energy conservation. The Newton's method used with the proposed schemes in the numerical tests has a tolerance of error of $1e-8$ and a max number of iteration of 20.

Table 2: A comparison of efficiencies of the ETDRK4, RK4 and Fourth-order conservative methods using LDG-C ($N=128$) on (5.1). (By choosing the following two time steps, the solutions of the three methods are comparable. We are trying to achieve errors of the similar orders.)

T	ETDRK4 ($\tau=0.1$)		RK4 ($\tau=0.0001$)		Fourth-order conservative ($\tau=0.1$)	
	CPU time	L_2 error	CPU time	L_2 error	CPU time	L_2 error
5	3.0436	9.3566e-007	20.1372	2.5194e-006	6.88e+003	3.5463e-006
10	4.6826	5.6233e-006	33.1450	4.3198e-005	1.21e+004	7.0926e-006
20	7.7688	3.6756e-005	47.9093	9.0924e-005	2.19e+004	1.4185e-005
30	10.9177	9.6743e-005	60.2801	3.0351e-004	3.26e+004	2.1278e-005

Table 2 presents the advantage in efficiency of the ETDRK4. We can observe that the ETDRK4 achieves more accurate results than RK4 and the Fourth-order conservative method (4.5) with less CPU time. The CPU times are based on computations via Matlab 7.9.0 platforms based on an Intel Core i5-2410M 2.30GHz workstation.

5.2 2-coupled NLSE

Consider the following 2-coupled NLSE [36]

$$\begin{aligned} iu_{1t} + i\alpha u_{1x} + u_{1xx} + (|u_1|^2 + \beta|u_2|^2)u_1 &= 0, \\ iu_{2t} - i\alpha u_{2x} + u_{2xx} + (\beta|u_1|^2 + |u_2|^2)u_2 &= 0, \end{aligned} \quad (5.3)$$

with following initial conditions

$$\begin{aligned} u_1(x,0) &= \sqrt{\frac{2a}{1+\beta}} \operatorname{sech}(\sqrt{2a}(x-x_0)) \exp(i(c-\alpha)(x-x_0)), \\ u_2(x,0) &= \sqrt{\frac{2a}{1+\beta}} \operatorname{sech}(\sqrt{2a}(x-x_0)) \exp(i(c+\alpha)(x-x_0)), \end{aligned} \quad (5.4)$$

as well as periodic boundary conditions in $[-25, 25]$, where $a=1$, $c=1$, $\alpha=0.5$, $\beta=\frac{2}{3}$ and $x_0=0$. Exact solutions to (5.3) with initial and boundary conditions (5.4) are given in [36]:

$$\begin{aligned} u_1(x,t) &= \sqrt{\frac{2a}{1+\beta}} \operatorname{sech}(\sqrt{2a}(x-ct)) \exp\left(i\left((c-\alpha)x - \left(\frac{c^2-\alpha^2}{2} - a\right)t\right)\right), \\ u_2(x,t) &= \sqrt{\frac{2a}{1+\beta}} \operatorname{sech}(\sqrt{2a}(x-ct)) \exp\left(i\left((c+\alpha)x - \left(\frac{c^2-\alpha^2}{2} - a\right)t\right)\right). \end{aligned} \quad (5.5)$$

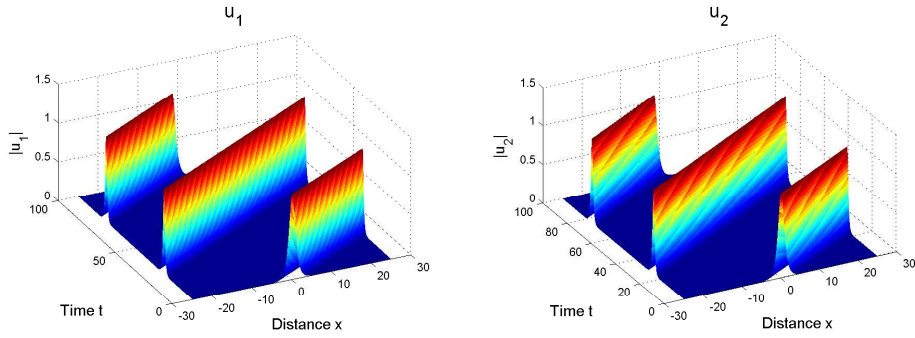


Figure 8: Surface plots of results by the ETDRK4 solving 2-coupled NLSE (5.3) with initial condition (5.4) and periodic boundary condition using LDG-C in space ($N=128$ and $\tau=0.1$).

To observe the convergence rate of ETDRK4 in Fig. 9 we set $N=512$ to make sure that the LDG-C is accurate enough in space and then we change τ and compute the corresponding L_2 error of u_1 and u_2 . The slopes of the regression lines indicate the ETDRK4 is fourth order solving the 2-coupled NLSE. In a similar way we fix $\tau=0.1$ and record the

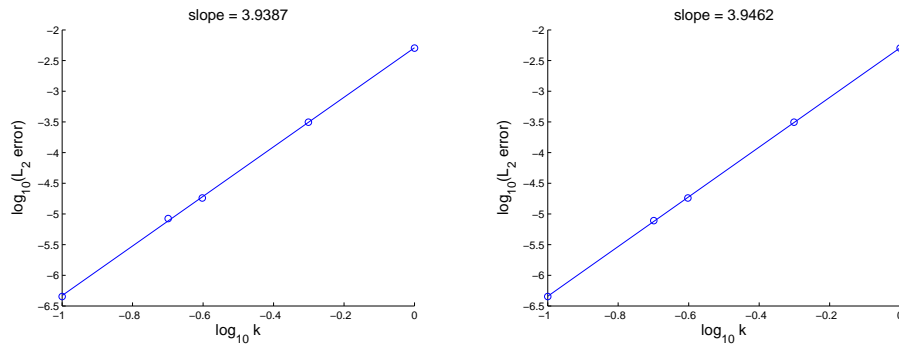


Figure 9: Convergence rates of the ETDRK4 solving 2-coupled NLSE (5.3) with initial and boundary conditions provided using LDG-C in space ($N=512$). Results of u_1 on the left and results of u_2 on the right.

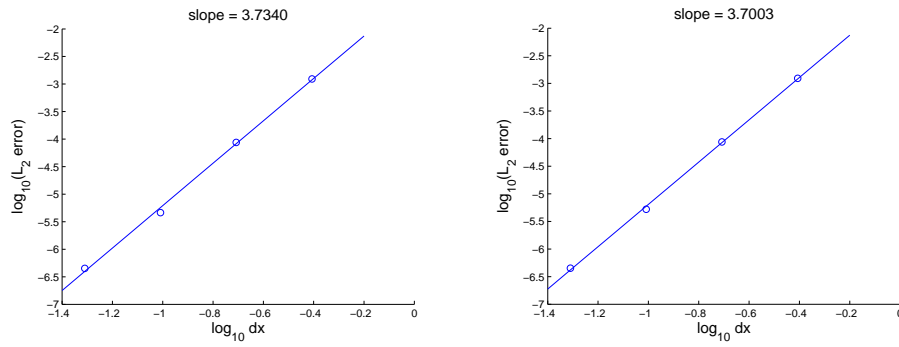


Figure 10: Convergence rates of the LDG-C solving 2-coupled NLSE (5.3) with initial and boundary conditions provided using ETDRK4 in time ($\tau=0.1$). Results of u_1 on the left and results of u_2 on the right.

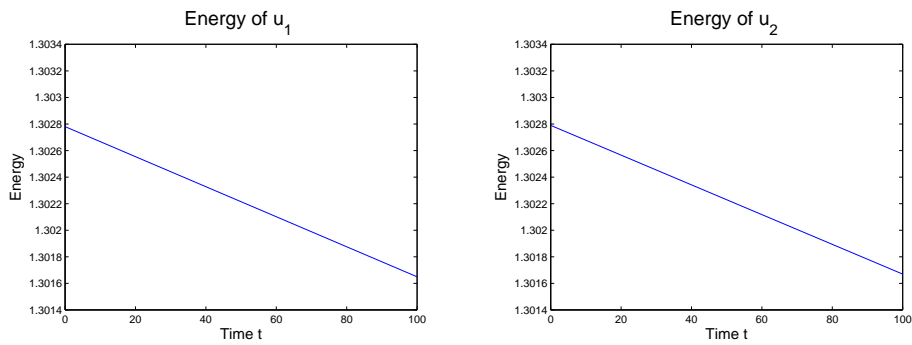


Figure 11: Energy of results by the ETDRK4 solving 2-coupled NLSE (5.3) with initial and boundary conditions provided using LDG-C in space ($N=128$ and $\tau=0.1$).

L_2 error by changing dx . The slopes of the regression lines in Fig. 10 correspond to the fact that LDG-C is a fourth order method in space.

The Energy of the numerical solution u can be conveniently evaluated via the spectral norm $\|u\|_2$. We notice from Fig. 11 that the energy of u_1 and u_2 decreases almost linearly, and very slowly, as time goes from 0 to 100. This result indicates the ETDRK4 will not have a blow-up solution even after a long-time period of calculation, which is better than some explicit temporal discretization.

Interaction of two solitons Next, we consider the following 2-coupled NLSE [20]

$$\begin{aligned} iu_{1t} + i\delta u_{1x} + \frac{1}{2}u_{1xx} + (|u_1|^2 + e|u_2|^2)u_1 &= 0, \\ iu_{2t} - i\delta u_{2x} + \frac{1}{2}u_{2xx} + (e|u_1|^2 + |u_2|^2)u_2 &= 0, \end{aligned} \quad (5.6)$$

with the initial conditions

$$\begin{aligned} u_1(x,0) &= \sum_{j=1}^2 \sqrt{\frac{2a_j}{1+e}} \operatorname{sech}(\sqrt{2a_j}x_j) \exp i((v_j - \delta)x_j), \\ u_2(x,0) &= \sum_{j=1}^2 \sqrt{\frac{2a_j}{1+e}} \operatorname{sech}(\sqrt{2a_j}x_j) \exp i((v_j + \delta)x_j), \end{aligned} \quad (5.7)$$

where $\delta = 0.2, e = 2/3, x_1 = x, x_2 = x - 25, x_L = -20, x_R = 80, v_1 = 1, v_2 = 0.1, a_1 = 1, a_2 = 0.5$ and periodic boundary conditions in $[x_L, x_R]$.

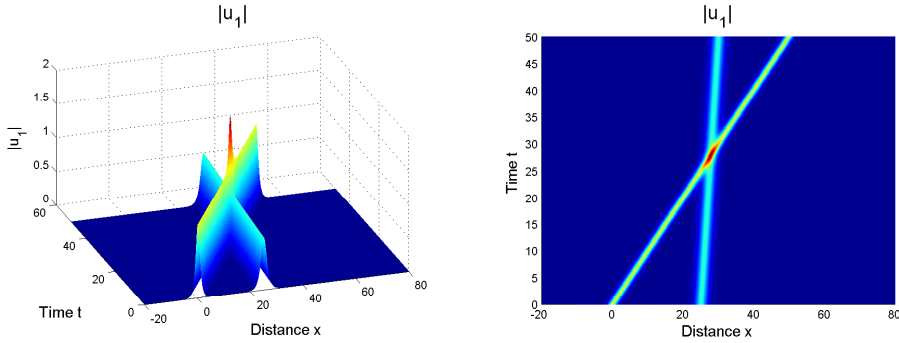


Figure 12: Surface plots of results by the ETDRK4 solving 2-coupled NLSE (5.6) with initial condition (5.7) and periodic boundary condition using LDG-C in space ($N=128$ and $\tau=0.1$).

The surface plots of $|u_1|$ and $|u_2|$ are identical for interaction of two solitons, thus we only represent $|u_1|$ here. We notice from Fig. 12 that the two solitons travel to the right at velocities 1 and 0.1. They interact at about $t = 30$ and do not affect each other.

The energy of solutions in Table 3 indicates the ETDRK4 using LDG-C conserves the energy well for this problem. Comparing with Newton's method using finite difference provided by [20], the ETDRK4 using LDG-C has smaller errors in energy for the long time simulation. We compare with Newton's method since it is supposed to behave well in energy conservation for a long time simulation.

Table 3: A comparison of energy by ETDRK4 using LDG-C and Newton's method using finite difference on (5.6) and (5.7) ($dx=0.2, \tau=0.1$).

T	ETDRK4	Newton's method [20]
0	1.702074	1.702074
10	1.702074	1.702074
20	1.702074	1.702074
30	1.702074	1.702073
40	1.702069	1.702064
50	1.702021	1.701613

Interaction of three solitons For 2-coupled NLSE (5.6), we use the initial conditions

$$\begin{aligned}
 u_1(x,0) &= \sum_{j=1}^3 \sqrt{\frac{2a_j}{1+e}} \operatorname{sech}(\sqrt{2a_j}x_j) \exp i((v_j - \delta)x_j), \\
 u_2(x,0) &= \sum_{j=1}^3 \sqrt{\frac{2a_j}{1+e}} \operatorname{sech}(\sqrt{2a_j}x_j) \exp i((v_j + \delta)x_j),
 \end{aligned} \tag{5.8}$$

where $\delta=0.5, e=2/3, a_1=1.2, a_2=0.72, a_3=0.36, v_1=1, v_2=0.1, v_3=-1, x_1=x, x_2=x-25, x_3=x-50, x_L=-20, x_R=80$ and periodic boundary conditions in $[x_L, x_R]$.

The surface plots of $|u_1|$ and $|u_2|$ are identical for interaction of three solitons, thus we only represent $|u_1|$ here. We notice from Fig. 13 that the three solitons travel at velocities 1, 0.1 and -1 along x direction. They interact between $t=20$ and $t=30$ and do not affect each other. The energy of solutions in Table 4 indicates the ETDRK4 using LDG-C conserves the energy well for this problem. Comparing with Newton's method using finite difference provided by [20], the ETDRK4 using LDG-C achieves energy with errors of the same orders.

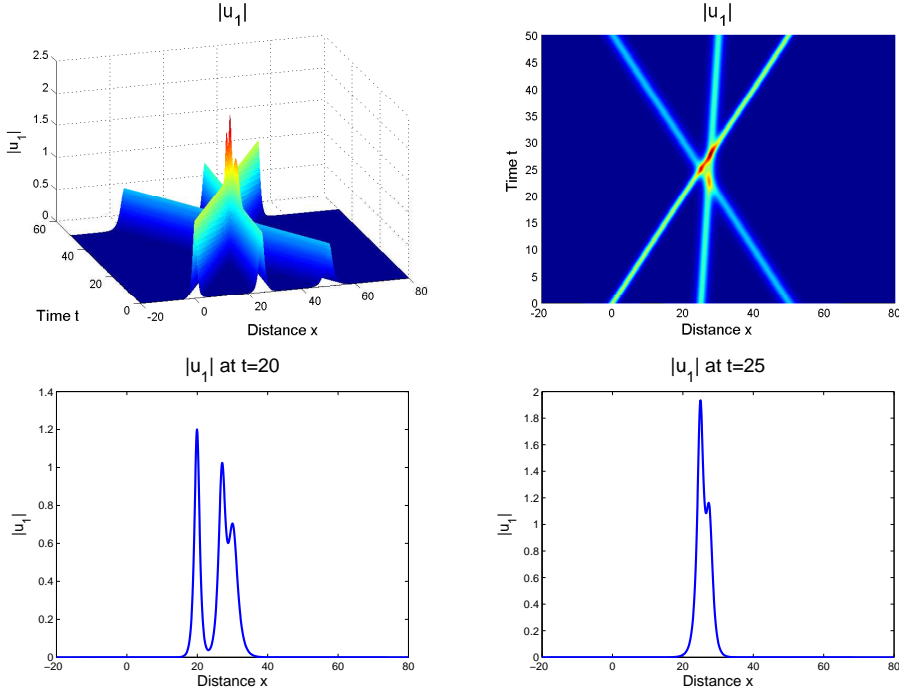


Figure 13: Surface plots of results by the ETDRK4 solving 2-coupled NLSE (5.6) with initial condition (5.8) and periodic boundary condition using LDG-C in space ($N=128$ and $\tau=0.1$).

Table 4: A comparison of energy by ETDRK4 using LDG-C and Newton's method using finite difference on (5.6) and (5.8) ($dx=0.2$, $\tau=0.1$).

T	ETDRK4	Newton's method [20]
0	2.077803	2.077803
10	2.077803	2.077803
20	2.077802	2.077803
30	2.077801	2.077802
40	2.077801	2.077802
50	2.077802	2.077803

5.3 4-coupled NLSE

In the last subsection, we consider the following 4-coupled NLSE, see as well in [1],

$$\begin{aligned}
 iu_{1t} + i\frac{1}{v_1}u_{1x} + \frac{\beta_1}{2}u_{1xx} + \gamma_1(|u_1|^2 + 2|u_2|^2 + B|u_3|^2 + B|u_4|^2)u_1 &= 0, \\
 iu_{2t} + i\frac{1}{v_2}u_{2x} + \frac{\beta_2}{2}u_{2xx} + \gamma_2(2|u_1|^2 + |u_2|^2 + B|u_3|^2 + B|u_4|^2)u_2 &= 0, \\
 iu_{3t} + i\frac{1}{v_3}u_{3x} + \frac{\beta_1}{2}u_{3xx} + \gamma_1(B|u_1|^2 + B|u_2|^2 + |u_3|^2 + 2|u_4|^2)u_3 &= 0, \\
 iu_{4t} + i\frac{1}{v_4}u_{4x} + \frac{\beta_2}{2}u_{4xx} + \gamma_2(B|u_1|^2 + B|u_2|^2 + 2|u_3|^2 + |u_4|^2)u_4 &= 0,
 \end{aligned} \tag{5.9}$$

with the initial conditions

$$\begin{aligned}
 u_1(x,0) &= \sqrt{\frac{2a}{1+B}} \operatorname{sech}(\sqrt{2a}(x-x_0)) \exp(i(c-\alpha)(x-x_0)), \\
 u_2(x,0) &= \sqrt{\frac{2a}{1+B}} \operatorname{sech}(\sqrt{2a}(x-x_0)) \exp(i(c+\alpha)(x-x_0)), \\
 u_3(x,0) &= \sqrt{\frac{2a}{1+B}} \operatorname{sech}(\sqrt{2a}(x-x_0)) \exp(i(c-\alpha)(x-x_0)), \\
 u_4(x,0) &= \sqrt{\frac{2a}{1+B}} \operatorname{sech}(\sqrt{2a}(x-x_0)) \exp(i(c+\alpha)(x-x_0)),
 \end{aligned} \tag{5.10}$$

as well as periodic boundary conditions in $[-10, 40]$, where $v_1=v_2=v_3=v_4=1$, $\beta_1=\beta_2=2$, $\gamma_1=\gamma_2=2$, $a=1$, $c=1$, $\alpha=0.5$, $B=\frac{2}{3}$ and $x_0=0$.

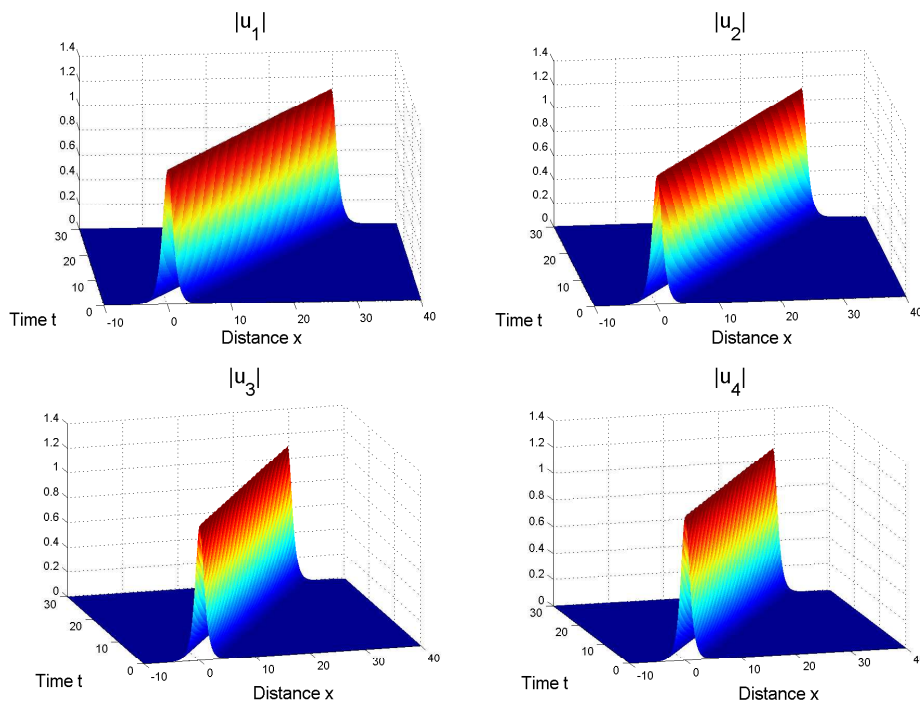


Figure 14: Solutions of the 4-coupled NLSE (5.9) with initial conditions (5.10) obtained via the ETDRK4 LDG-C method ($h=0.1$, $\tau=0.1$ and $t=[0,30]$.)

As explained in [1], the four-coupled NLSE equations can be used in modeling solitons in the high-birefringence fibers. The parameter B equals $2/3$ for linearly birefringent fibers, and β_1, β_2 are the corresponding propagation constant.

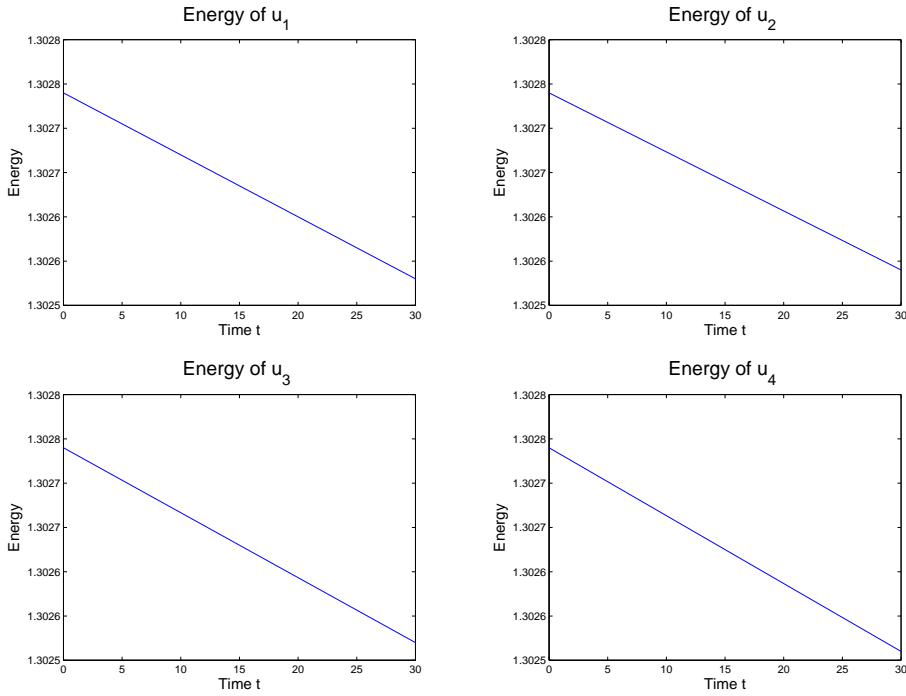


Figure 15: Time history of the energy of the 4-coupled NLSE (5.9) with initial conditions (5.10) obtained via the ETDRK4 LDG-C method ($h=0.1$, $\tau=0.1$ and $t=[0,30]$.)

We run the simulation for the coupled NLSE with the fourth order ETDRK4 LDG-C method. The numerical results are shown in Fig. 14. We observe that the numerical results of (5.9) are soliton waves that travel along the x -direction at a speed of 1. The time history of energy, plotted in Fig. 15, indicates the energy of numerical results by ETDRK4 will decrease slightly as time goes. This numerical test demonstrates that the ETDRK4 LDG-C method works well on large systems of NLSEs.

6 Conclusion and Future Work

We have developed and analyzed an LDG approximation based ETDRK4 method for solving the underlying N -coupled NLSEs. The accuracy, efficiency and stability of the numerical method are discussed. It has been evident from the analysis and numerical results that the method is highly efficient and reliable. Future work includes continuing developments of highly accurate exponential time differencing strategies and the adaptive mesh designs for the multidimensional coupled NLSEs.

Acknowledgments

Research of Y. Xing is sponsored by NSF grant DMS-1216454, Oak Ridge National Laboratory (ORNL) and the U. S. Department of Energy, Office of Advanced Scientific Computing Research. The work was partially performed at ORNL, which is managed by UT-Battelle, LLC, under Contract No. DE-AC05-00OR22725.

References

- [1] Agrawal G. P.: *Nonlinear Fiber Optics*, 264-267. Academic Press (2001)
- [2] Anderson D.: Variational approach to nonlinear pulse propagation in optical fibers, *Phys. Rev. A*, 3rd Series, 3135-3145 (1983)
- [3] Benney D.J., Newll A.C.: The propagation of nonlinear wave envelopes, *J. Math. Phys.* 46, 133139 (1967)
- [4] Berland H., Islas A. L., Schober C.M.: Solving the nonlinear Schrödinger equation using exponential integrators, *J. Comput. Phys.*, 255, 284-299 (2007)
- [5] Beylkin G., Keiser J. M., Vozovoi L.: A new class of time discretization schemes for the solution of nonlinear PDEs, *J. Comput. Phys.*, 147, 362-387 (1998)
- [6] Bona J.L., Chen H., Karakashian O., Xing Y.: Conservative discontinuous Galerkin methods for the Generalized Korteweg-de Vries equation. *Mathematics of Computation*, 82, 1401-1432 (2013)
- [7] Chang Q.S., Jia E. and Sun W.: Difference schemes for solving the generalized nonlinear Schrödinger equation, *Journal of Computational Physics*, 148, 397-415 (1999)
- [8] Cheng Y., Shu C.-W.: Superconvergence of discontinuous Galerkin and local discontinuous Galerkin schemes for linear hyperbolic and convection diffusion equations in one space dimension, *SIAM J. Numer. Anal.*, 47, 4044-4072 (2010)
- [9] Chou C.-S. , Shu C.-W., Xing Y.: Optimal energy conserving local discontinuous Galerkin methods for second-order wave equation in heterogeneous media, *Journal of Computational Physics*, 272, 88-107 (2014)
- [10] Ciarlet P. G.: *The Finite Element Method for Elliptic Problems*, North-Holland, Amsterdam (1978)
- [11] Cockburn B. , Shu C.-W.: TVB Runge-Kutta local projection discontinuous Galerkin finite element method for conservation laws II: general framework. *Mathematics of Computation*, 52, 411-435 (1989)
- [12] Cockburn B. , Shu C.-W.: The local discontinuous Galerkin method for time-dependent convection-diffusion systems. *SIAM J. Numer. Anal.*, 35, 2440-2463 (1998)
- [13] Cockburn B. , Shu C.-W.: Runge-Kutta discontinuous Galerkin methods for convection-dominated problems. *Journal of Scientific Computing*, 16, 173-261 (2001)
- [14] Cox S. M., Matthews P. C.: Exponential time differencing for stiff systems, *J. Comput. Phys.*, 176, 430-455 (2002)
- [15] Griffiths D. F., Mitchell A. R., Morris J. L.: A numerical study of the nonlinear Schrödinger equation, *Comput. Methods in Appl. Mech. Eng.*, 45, 177-215 (1984)
- [16] Hederi M., Islas A. L., Reger K., Schober C.M.: Efficiency of exponential time differencing schemes for nonlinear Schrödinger equations, *Math. Comput. Simulat.*, (2013), <http://dx.doi.org/10.1016/j.matcom.2013.05.013>
- [17] Hochbruck M., Ostermann A.: Exponential integrators, *Acta Numerica.*, 209-286 (2010)

- [18] Hoz F. D., Vasillo F.: An exponential time differencing method for the nonlinear Schrödinger equation, *Comput. Phys. Commun.*, 179, 449-456 (2008)
- [19] Ismail M. S., Alamri S. Z.: Highly Accurate Finite Difference Method for Coupled Nonlinear Schrödinger equation, *Int. J. Comp. Math.* 81, 333C351 (2004)
- [20] Ismail M. S. , Taha T. R.: Numerical simulation of coupled nonlinear Schrödinger equation, *Math. Comput. Simulat.*, 56, 547-562 (2001)
- [21] Karakashian O. and Makridakis C.: A spacetime finite element method for the nonlinear Schrödinger equation: the discontinuous Galerkin method, *Mathematics of Computation*, 67, 479-499 (1998).
- [22] Kassam A-K., Trefethen L. N.: Fourth-order time-stepping for stiff PDEs, *SIAM J. Sci. Comput.*, 26, 1214-1233 (2005)
- [23] Klein C.: Fourth order time-stepping for low dispersion Korteweg-De Vries and nonlinear Schrödinger equations, *Electron. Trans. Numer. Anal.*, 29, 116-135 (2008)
- [24] Khaliq A. Q. M., Martin-Vaquero J., Wade B.A., Yousuf M.: Smoothing schemes for reaction-diffusion systems with non-smooth data. *J. Comput. Appl. Math.*, 223, 374-386 (2009)
- [25] Lange H.: On Dysthe's nonlinear Schrödinger equation for deep water waves, *Transp. Theory Stat. Phys.*, 29, 509-524 (2000)
- [26] Liang X., Khaliq A. Q. M., Sheng Q.: Exponential time differencing Crank-Nicolson method with a quartic spline approximation for nonlinear Schrödinger equations, *Appl. Math. Comp.*, 235, 235-252 (2014)
- [27] Meng X. , Shu C.-W., Wu B.: Optimal error estimates for discontinuous Galerkin methods based on upwind-biased fluxes for linear hyperbolic equations, submitted to *Mathematics of Computation*
- [28] Menyuk C. R.: Nonlinear pulse propagation in birefringent optical fibers, *IEEE J. Quantum Electron.* QE-23, 174-176 (1987)
- [29] Pathria D. and Morris J.L.: Pseudo-spectral solution of nonlinear Schrödinger equations, *Journal of Computational Physics*, 87, 108-125 (1990).
- [30] Sanz-Serna J. M., Verwer J. G.: Conservative and nonconservative schemes for the solution of the nonlinear Schrödinger equation, *IMA J. Numer. Anal.*, 6, 25-42 (1986)
- [31] Sulem P. L., Sulem C., Patera A.: Numerical simulation of singular solutions to the two-dimensional cubic Schrödinger equation, *Pure Appl. Math.*, 37, 755-778 (1984)
- [32] Sheng Q., Khaliq A.Q.M. and Al-Said E.A.: Solving the generalized nonlinear Schrödinger equation via quartic spline approximation, *Journal of Computational Physics*, 166, 400-417 (2001).
- [33] Sun Z. Z., Zhao D. D. : On the L_∞ convergence of a difference scheme for coupled nonlinear Schrödinger equations, *Comput. Math. Appl.*, 59, 3286-3300 (2010)
- [34] Taha T.R. and Ablowitz M.J.: Analytical and numerical aspects of certain nonlinear evolution equations II. Numerical, nonlinear Schrödinger equation, *Journal of Computational Physics*, 55, 203-230 (1984).
- [35] Xing Y, Chou C.-S., and Shu C.-W.: Energy conserving local discontinuous Galerkin methods for wave propagation problems. *Inverse Problems and Imaging*, 7, 967-986 (2013)
- [36] Xu Y. , Shu C.-W.: Local discontinuous Galerkin methods for nonlinear Schrödinger equations, *J. Comput. Phys.*, 205, 72-97 (2005)
- [37] Xu Y., Shu C.-W.: Optimal error estimates of the semi-discrete local discontinuous Galerkin methods for high order wave equations, *SIAM Journal on Numerical Analysis*, 50, 79-104 (2012)
- [38] Xia Y., Xu Y. , Shu C.-W.: Efficient time discretization for local discontinuous Galerkin meth-

ods, Discret. Contin. Dyn. S. – Series B, 8, 677-693 (2007)